Accurate and Efficient Numerical Solution for Trans-critical Steady Flow in a Channel with Variable Geometry

SAEED-REZA SABBAGH-YAZDI [*], BEHZAD SAEEDIFAR [**]
Civil Engineering Department,
KN Toosi University of Technology,
No.1346 Valiasr Street, 19697- Tehran
IRAN

and

NIKOS E. MASTORAKIS [***]
Military Insitutes of University Education (ASEI)
Hellenic Naval Academy
Terma Chatzikyriakou 18539,
Piraues, GREECE

Abstract: - The goal of this work is to extend finite volume schemes to the hyperbolic balance laws with geometrical source term. Mixed regions of flow are considered when a super-critical to sub-critical transition takes place and hydraulic jumps occur. In this work, the shallow water equations are used to solve the open-channel flow. The equations are converted to discrete form using cell centre finite volume method for triangular unstructured meshes. For obtaining stable numerical solution, the biharmonic operator that can be computed in some certain computational stages, but its value adds to the equations in all computational steps. For preventing excessively long run times, local time stepping is used, whereby the computations on individual cells are advanced by their own maximum allowable time steps. Using cell center finite volume method for discrete formulations, proper algorithm is adopted for accurate numerical solution by considering grids, boundary conditions transferring information between nodes and centeroids of cells.
The accuracy of the computed results is validated by modeling mixed sub and super critical flow in a channel with variable bottom elevation and width. Comparison of the computed water elevation with analytical solution obtained from the theoretical solution for the frictionless free surface flow shows encouraging agreements.

Key-Words: - Cell Center Finite Volume Method; Shallow Water Equations; Open-Channel Flow; Unstructured Triangular Mesh

1 Introduction

A number of problems can be identified with the software currently available, and as a result, research continues into developing better numerical techniques for computational hydraulics. There has been a growing trend in favor of Riemann based methods constructed within the finite volume framework. However, the computational cost of employing this algorithm can lead to excessively long run times, particularly when higher order mathematical models are used. This often is as a result of stability constraints placed upon explicit schemes, which require the smallest possible time step permitted throughout the grid, to be applied globally.
The application of faster and more accurate numerical methods is considered by researchers therefore one possibility for improving this situation is to use local time stepping, whereby individual cells are advanced by their own maximum allowable time steps. To incorporate this concept into a transient model requires the development of a suitable integration strategy, to ensure that the solution remains accurate in time. Many techniques are available for numerical simulation work, such as Finite Difference methods (FDM), Finite Element methods (FEM), Spectral methods and Finite Volume methods (FVM). Within the context of open channel flows, earlier worked focused on the application of finite difference schemes and to some extent the finite element method.
There are numerous finite difference schemes for spatial discretisation. They can be divided into two broad categories; central difference schemes and

upwind schemes. Central difference schemes have higher order accuracy but more restrictive stability requirement and tend to generate spurious oscillations. Upwind schemes on the other hand are generally more stable due to inherent dissipation effects at the price of lower order accuracy.

In more recent studies, finite volume method has become the more popular approach for general fluid flow problems. This method is based on the integral form of the conservation equations [27].

Several techniques have been published in the literature concerning the use of the finite volume method to solve the two-dimensional (2-D) shallow water equations to model free surface flows. Zhao et al. [28,29] used three-types of Riemann solvers, including the flux vector splitting, the flux difference splitting and the Riemann solver of Osher and Solomone [21].

Anastasiou and Chan [1,3] developed a finite volume scheme based on a Godunov-type second-order upwind formulation to solve incompressible flows, both with and without a free surface and using an unstructured triangular mesh. Mingham and Causon [19] developed a high resolution finite volume scheme using a MUSCL reconstruction and with a slope limiter to capture surface discontinuities. Their model was applied to simulate bore wave diffraction in both internal and external hydraulic flows. More recently Lin et al. [16] have proposed an algorithm based on the flux-splitting technique. The algorithm was established by modifying the MacCormack scheme to preserve second-order accuracy of the numerical algorithm.

Nelida Crnjaric _Zic and Senka Vukovic [20] proposed the Balanced finite volume WENO and central WENO schemes to solve selected test case that discussed later.

WENO (Weighted Essentially Non-Oscillatory) schemes are based on the ENO (Essentially Non-Oscillatory) schems of Harten (1983) [7] and Harten et al (1987) [8].

The key idea of ENO scheme is to use the smoothed stencil among several candidates to approximate flux at cell boundaries $(i \pm 1/2)$ to high order and at the same time to avoid spurious oscillations near shocks or discontinuities. WENO schemes take one step further by taking weighted average of the candidate stencils. Weights are adjusted by local smoothness. More details can be found in Liu et al (1994)[15], Jiang and Shu (1996)[11], Jiang et al (1999)[12] and Shao et al (2004)[23].

Vaserio Caleffi, Alessandro Valiani and Andrea Zanni, (2003)[26], developed 2D computer code for solving , flow in a channel with variable height. Their algorithm was obtained through the spatial discretisation of the shallow water equations by a cell center finite volume method, based on the Godunov approach. The Harten, Lax and Van Leer (HLL) Riemann solver was used. A second order accuracy in space and time was achieved, respectively by MUSCL and predictor–corrector techniques. The high resolution requirement was ensured by satisfaction of TVD property.

In this paper, accurate and efficient of the cell center finite volume solution by computation of fluxes at boundary of the triangular control volume using the variables at centroids of two adjacent cells. Particular attention was posed to the numerical treatment of source terms for solving steady flow in a channel with variable bed topography and channel width is considered. In order to handle the variable geometry of the flow field, unstructured triangular mesh has been deployed to cover the solution domain. A test case of trans-critical flow in a frictionless channel with variable geometry [17] is chosen to check the developed flow solver.

2 Governing Equations

The hydrodynamic module is based on the solution of the two-dimensional Shallow Water Equations (SWE), whit assumption the incompressible water, described as:

2.1. Conservation of Mass and Momentum

This property of SWE was accurately investigated in several works; for a review, look at Toro [24] and Morris [18]. Theoretical bases of the SWE theory may be found in Liggett [14] and Chaudhry [4]. Cunge et al [5] (see also [9]).

The dependent flow variables in such equations are the flow depth (h) and the x and y components of the unit discharge (hu and hv), related to the corresponding vertically averaged flow velocity components (u and v).

2.1.1. Conservation of Mass: The law of conservation of mass states that mass can neither be destroyed nor created, but it can only be transformed by physical, chemical or biological processes. All mass flow rates into a control volume through its control surface is equal to all mass flow rates out of the control volume plus the time change in mass inside the control volume.

$$\frac{\partial h}{\partial t} + \frac{\partial hu}{\partial x} + \frac{\partial hv}{\partial y} = 0$$

2.1.2. Conservation of Momentum: It describes the motion of a flow particle at any time at any given position in the flow field.

$$\frac{\partial hu}{\partial t}+\frac{\partial}{\partial x}(hu^2)+\frac{\partial}{\partial y}(huv)=-gh\frac{\partial}{\partial x}(h+z_b)$$

$$\frac{\partial hv}{\partial t}+\frac{\partial}{\partial x}(huv)+\frac{\partial}{\partial y}(hv^2)=-gh\frac{\partial}{\partial x}(h+z_b)$$

Where, *t*: time; *x* and *y* horizontal Cartesian coordinates, *g*: gravitational acceleration. The complex turbulence effects are not included in the equations.

The shallow water equations are written in conservation form. One of the more common forms of the equations encountered within the literature is written as:

$$Q=\begin{bmatrix}h & hu & hv\end{bmatrix}^T \quad (1)$$

$$\frac{\partial Q}{\partial t}+\nabla\cdot F=S \quad (2)$$

where $F=F(Q)=\left[E(Q),G(Q)\right]$ is the flux vector and S is the source term as:

$$E=\begin{bmatrix}hu\\ hu^2\\ huv\end{bmatrix},\quad G=\begin{bmatrix}hv\\ hvu\\ hv^2\end{bmatrix},\quad S=\begin{bmatrix}0\\ -gh\,\partial\eta/\partial x\\ -gh\,\partial\eta/\partial y\end{bmatrix}$$

The parameter $\eta=h+z_b$ indicates the water surface level.

3 Boundary and Initial Conditions

Careful treatment of the boundary conditions is essential in order to avoid unwanted numerical phenomena, such as artificial boundary layers, unstable discretisations and numerical diffusion, and to approximate the physical flow as well as possible.

Various types of boundary conditions are specified in the numerical model for flow and wall boundary conditions.

For internal sub-critical flows distinction between inflow and outflow boundaries may prevent computational conflicts. Following implementations are made at inflow and outflow boundaries.

At inflow boundary nodes, the components of the free stream velocity, *u* and *v*, are specified and the depth, h, is extrapolated from the inside domain.

At the outflow boundary nodes, the depth, *h*, is imposed and the velocity components, *u* and *v*, are extrapolated from the interior nodes of domain [6].

For wall boundary, free slip condition is implemented by setting the component of the velocity normal to the wall boundary equal to zero.

$(U.\hat{n})_w=0$ in which U is velocity vector and $\hat{n}$ is the normal vector perpendicular to the wall boundary.

4 Numerical Formulation

An important factor in applying numerical techniques is the question of grid generation.

An unstructured triangular mesh has been deployed to cover the solution domain and enable arbitrary and complex geometries to be replicated.

In a finite volume cell centred grid, each triangle is considered as a control volume and the computed variables are considered to locate at its centroid, so that the number of unknown vectors is the same as the number of elements or triangles.

The finite volume method is based on writing the mathematical model equations in integral form over an elementary control volume. Each elementary volume is represented by a cell of the mesh, used for the discretisation of the simulated domain.

Equation (2) can be integrated over the cell volume Ω as:

$$\int_\Omega\frac{\partial Q}{\partial t}dx.dy+\int_\Omega\nabla\cdot Fd\Omega=\int_\Omega S.d\Omega \quad (3)$$

The continuity and the momentum equations are integrated over each control volume. Application of the Green's theorem to the integrated continuity and momentum equation result are:

$$\Delta Q=-\frac{\Delta t}{\Omega_i}\left[\oint_\Gamma\overline{E}\cdot dy-\oint_\Gamma\overline{G}\cdot dx\right]+S_i\cdot\Delta t \quad (4)$$

Where Ω_i and Γ are the area and boundaries of the control volume, respectively.

The integral discretisation of the flux through the whole surface boundary of the control volume is obtained by the introduction of a sum, over the tree sides of each element and describe as:

$$Q^{n+1}=Q^n-\frac{\Delta t}{\Omega_i}\left[\sum_{i=1}^{3}(\overline{E}\cdot\Delta y-\overline{G}\cdot\Delta x\right]+S_i\Delta t \quad (5)$$

Where Q^n is the known value of *Q* while, Q^{n+1} is the value of *Q* to be computed after Δt. *S* is body forces of two equations of motion and equal to zero for continuity equation.

The parameters $\overline{E}$ and $\overline{G}$ are the averaged values of the fluxes in *x* and *y* spatial derivatives in each centre at the two side boundary edges of the control volume (Figure 1). S is the known values of parameters in right hand of equation 2 and equal to zero for continuity equation.

The special derivatives of source terms (which present water surface level $h+z_b$ gradients in x and

y directions at cell centroids) are computed over triangular control volumes using following formula:

$$S_x = -g\bar{h}\sum_{i=1}^{3}(\bar{h}+\bar{z})\Delta y\,,\quad S_y = +g\bar{h}\sum_{i=1}^{3}(\bar{h}+\bar{z})\Delta x$$

Having computed these gradients, the computations of the source terms are completed by multiply them to $g\bar{h}$ at cell centeroids.

S_x and S_y is derivatives of source terms in *x* and *y* direction that consist effect of bed topography and depth average hydrostatic pressure.

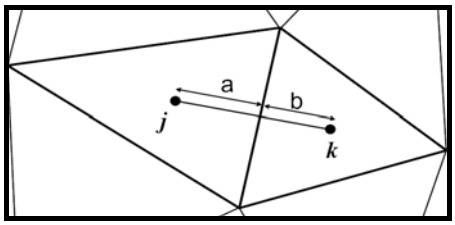

Fig. 1. Cells centroids of a control volume edge

However for the boundary (wall, inflow and out flow) edges in which the boundary conditions are imposed at their two end nodes, the fluxes are estimated using the variables at those nodes. For the other interior edges of the boundary cells, the effect of imposed boundary conditions at the boundary nodes are transferred to the cell centroids using weighted average reconstruction technique. Hence, before proceeding to the next time-step, all boundary variables ($Q = \begin{bmatrix} h & hu & hv \end{bmatrix}^T$) at centroids are updated, using following relation (Figure 2).

$$(Q_i)_{Centroid} = \frac{(Q_i)_{Node} \Big/ \sum_{i=1}^{3} d_i}{1 \Big/ \sum_{i=1}^{3} d_i} \qquad (6)$$

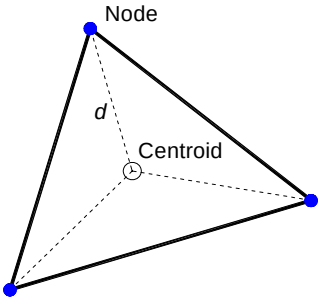

Fig. 2. Weighted average values of flow variables at a cell centroid

To prevent costly reconstruction of flow variables at computational nodes, the computed variables at cell centroids on two sides of the edges are averaged for estimating fluxes at control volume boundary edges.

In order to preserve the accuracy of the flux estimation by averaging, nearly non- stretched triangular meshes with $a \approx b$ (see Figure 1) are used in this work (Figure 3).

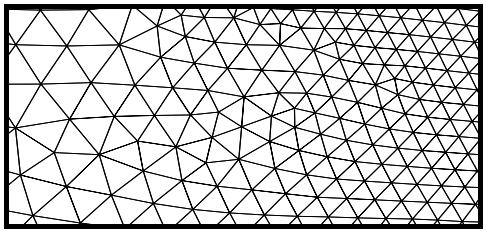

Fig. 3. variables on nearly non- stretched cells

It worth noting that, at the first time step the flow variables ($Q = \begin{bmatrix} h & hu & hv \end{bmatrix}^T$) for all centroids are transferred from the initial condition at computational nodes using the above mentioned weighted averaging formula for boundary cells.

5 Artificial Viscosity

For reducing computational efforts, the biharmonic operator can computed in some certain computational stages, but its value adds to the equations in all computational steps.

In order to stabilize the explicit solution procedure by damping out the numerical oscillations, a biharmonic artificial viscosity formulation can be added to above formulation. Considering the convictive fluxes as, $C(Q_i) = \sum_{i=1}^{3}(\overline{E}\cdot\Delta y - \overline{G}\cdot\Delta x)$ the fourth order artificial dissipation term, $D(Q_i) = \varepsilon\sum_{j=1}^{3}\lambda_{ij}(\nabla^2 Q_j - \nabla^2 Q_i)$ can be added to the aforementioned algebraic formulation. The scaling factor λ_{ij} is computed using the maximum central values of λ at the centre of neighbor cells that connected to the centre of the i control volume. λ is evaluated by $\lambda = \left|\vec{U}.\hat{n}\right| + \sqrt{\left|\vec{U}.\hat{n}\right|^2 + C^2\left(\Delta x^2 + \Delta y^2\right)}$, where $C = \sqrt{g\bar{h}}$ wit g is the gravity acceleration. Here, $\vec{U}$ is average central computed velocity at two neighbor cells that are common in edge for example edge a-b in Fig 1 and $\hat{n}$ is normal vectors at boundary edges of control volume Ω, respectively result in $\vec{U}.\hat{n} = \left|\bar{u}\Delta y - \bar{v}\Delta x\right|$. Depending on the sizes of grid spacing, the coefficient of the artificial dissipation term, ε should be tuned to the minimum required value ($1/256 \le \varepsilon \le 3/256$) for the applied mesh.

The algorithm for computation of artificial dissipation term is adopted for the unstructured mesh. Here, the Laplacian operator at every cell centers i, $\nabla^2 Q_i = \sum_{j=1}^{3}(Q_j - Q_i)$, is computed using the variable Q at centroid of desired cell i and centroids of its all neighboring cells j.
Finally, the revised fin
ite volume formula, which preserves the accuracy of the numerical solution, is written in the following form [10].

$$Q_i^{n+1} = Q_i^n - \frac{\Delta t}{\Omega_i}[C(Q_i) - D(Q_i)] + S_i \Delta t \qquad (7)$$

6 Time Stepping

For every control volume, Ω in computational domain, the time marching limit is specified as:

$$\Delta t = (CFL)\frac{\Omega}{\lambda} \qquad (8)$$

Where, parameter λ represents the maximum central values of Eigen-Values of Jacobin matrix of the convective dominated form of the equations at all centre of neighboring cells of the control volume and Ω is the control volume's area. The Courant-Fredrish-Levy number (CFL) is evaluated by the stability condition for explicit computation procedure. Since we are dealing with unstructured meshes, the size of control volumes varies over the computational domain. Therefore, every control volume has its own time step, Δt.
Kleb, Batina and Williams [13] presented a local time stepping technique for the Euler and Navier-Stokes equations on unstructured meshes.
The method was demonstrated through model validation, when supercritical to sub-critical flow transition problem is considered. Results for this test was good.
At final computational time marching, in order to define the flow variables ($Q = [h \quad hu \quad hv]^T$) at computational nodes, the values at centroids are transferred to the nodes using following relation (figure 4).

$$(Q_i)_{Node} = \sum_{i=1}^{N}(Q_i)_{Centroid} A_i \Big/ \sum_{i=1}^{N} A_i \qquad (9)$$

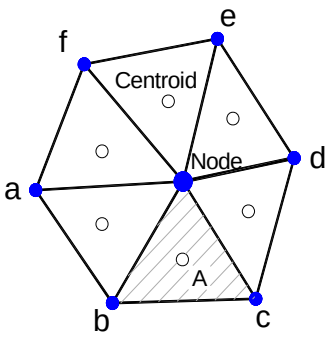

Fig. 4. Weighted average values of flow variables at a computational node

7 Model Validation

7.1. Test case1

The results of three tests on a channel are presented in this section. The aim of these test cases is to study the ability of the code to correctly represent the sub-critical, trans-critical and critical transition flow over a bump in a channel with variable height. For all three tests the channel geometry and flow conditions are the same as those are used by previous numerical workers [20, 25, 26]. The spatial domain is represented by a 25×1m rectangular cross section channel. The frictionless bottom elevation (z_b) of the channel is described by the following function:

$$z_f(x) = \begin{cases} 0.2 - 0{,}05(x-10)^2 & if\ 8m < x < 12 \\ 0 \qquad else & \end{cases}$$

The geometry of the channel and utilized unstructured mesh is plotted in following figure(5).

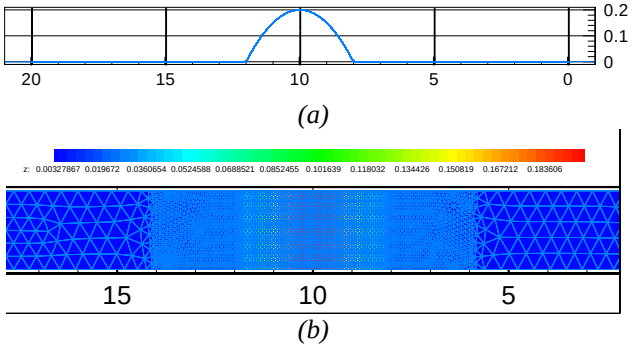

Fig. 5. The channel bed level (*a*) and bottom mesh colored by z (*b*)

7.1.1. Sub-critical flow over a bump

This test computes a transient flow, which tends to become a steady sub-critical flow. The imposed flow conditions at boundaries are $q_{in} = 4.42\, m^2/s$ and $h_{out} = 2m$. Figure 4 represents the computed water levels. Results of the developed model are

very close to the exact solution and the results of the previous numerical workers [20, 25, 26].

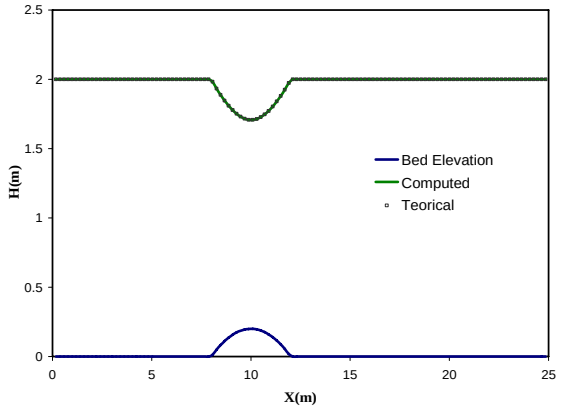

Fig. 4. Water elevation in sub-critical flow

7.1.2. Trans-critical flow over a bump

This test case forms a condition of sub-critical flow upstream of the bump and a supercritical flow downstream of the bump. The imposed conditions at flow boundaries for this test are $q_{in} = 1.53\, m^2/s$ and $h_{out} = 0.66m$.

Figure 5 shows acceptable result of the present algorithm for solution of trans-critical steady flow in comparison with the exact solution and the results of the previous numerical workers [20, 25, 26].

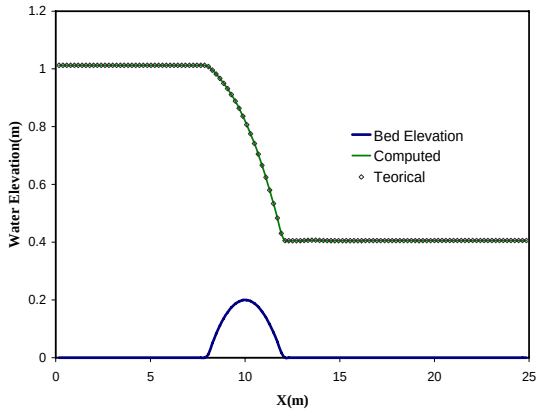

Fig. 5. Water elevation in trans-critical flow

7.1.3. Critical transition flow over a bump

For the third test, the upstream flow is considered $q_{in} = 0.18\, m^2/s$ and the downstream level is set equal to $h_{out} = 0.33m$. The analytical reference solution is obtained by application of Bernoulli's theorem.

Figure 6 shows a good agreement between the water profile, given by the analytical solution, the described numerical solution.

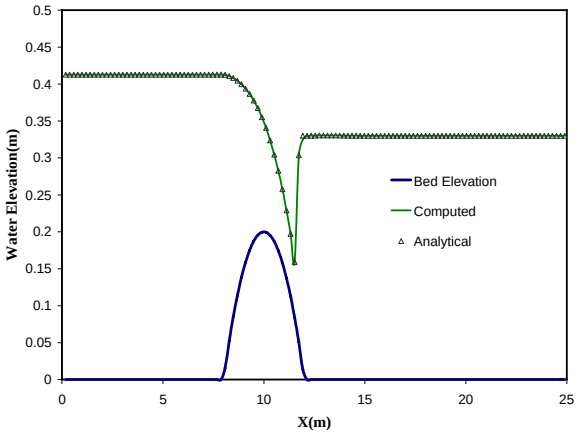

Fig. 6. Water elevation in critical transition flow:

7.2. Test case2

Steady flow in a channel with variable height and width is considered for testing the efficiency of the presented numerical scheme. The geometry for this test problem is taken from [17].

Hubbard and Garcia-Navarro [17] solved this test case using a complicated finite volume method. The channel bottom elevation and width are defined as (see Fig. 7).

$$z(x) = \begin{cases} 0.1\cos^2(\pi(x-1.5)) & if\ |x-1.5| < 0.5 \\ 0 & otherwise \end{cases}$$

and

$$B(x) = \begin{cases} 1-0.1\cos^2(\pi(x-1.5)) & if\ |x-1.5| < 0.5 \\ 0 & otherwise \end{cases}$$

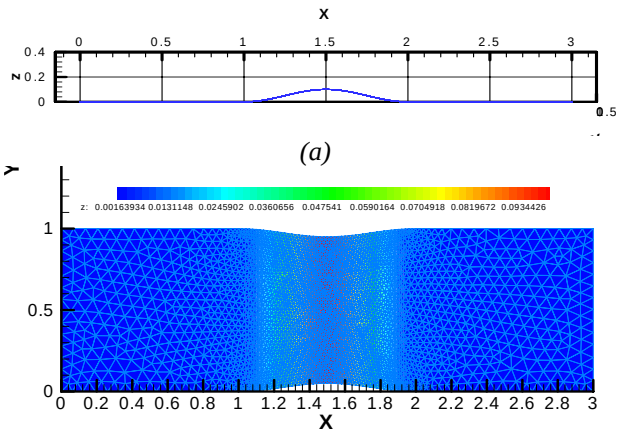

(a)

(b)

Fig. 7. The channel bed level (*a*) and bottom mesh colored by z presenting width variations (*b*)

For this test, the inflow discharge is considered as 1.88 m^3/s and the water depth of 1 m on downstream boundary is considered. Due to the variable bed elevation and width of the channel super-critical

flow forms at the point of the maximum contraction (which corresponds to the maximum bottom elevation), and then, it returns to the sub-critical regime. Therefore, at the critical point, a hydraulic jump forms down-stream of the bump.
The analytical reference solution of this case is obtained by application of Bernoulli's theorem [2]. Figure 8 shows the comparison of the results of the present flow solver with the analytical solution and the results of the previous numerical workers [17, 20].

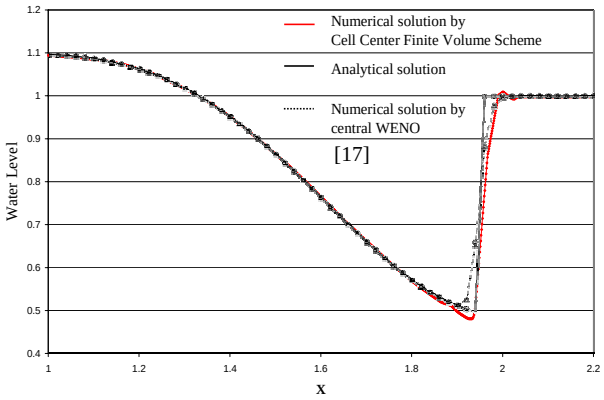

Fig. 8. Comparison of the numerical results, analytical solution and Previous Workers [17].

The comparison show encouraging agreements between the water level, given by the analytical solution, and the results of the present numerical algorithm.

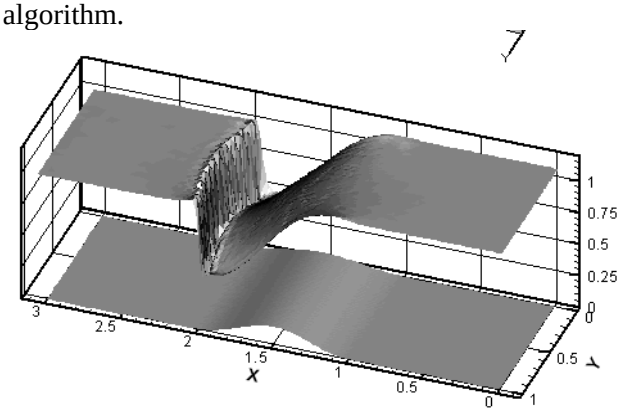

Fig. 9. Computed water surface and channel bottom

4 Conclusion

In this paper, a reconstruction free cell center finite volume algorithm for triangular unstructured meshed is introduced for solving convection dominated shallow water equations. In order to damp out the numerical noises associate with the explicit solution of the convective dominated (frictionless) flows, an artificial dissipation operator suitable for unstructured triangular meshes is added to center finite volume formulation. The accuracy of the algorithm a comparison between analytical solution and numerical results, obtained from the present finite volume algorithm, is presented.
In spite of the light computational work load of the present finite volume solver, its results its in close agreements with the exact solution of sub, super and trans-critical flow cases which are tested by costly numerical methods of the previous workers that mentioned above.

References:

[1] Anastasiou K, Chan CT. Solution of the 2D shallow water equations using the finite volume method on unstructured triangular meshes. *Int J Numer Methods Fluids 1997;24: 1225–45.*
[2] Bernoulli, D., *Hydrodinamica sive de viribus et motibus fluidorum commentarii*, Strasbourg (1738).
[3] Chan CT, Anastasiou K. Solution of incompressible flows with or without a free surface using the finite volume method on unstructured triangular meshes. *Int J Numer Methods Fluids 1999;29:35–57.*
[4] Chaudhry, MH., *Open-Channel Flow*, Prentice-Hall, Inc (1993).
[5] Cunge J. Holly F and Verwey A, *Practical aspect hydraulics*, Pitman Publishing Ltd, 1980
[6] Chaudhry, M. H.& Younus M., A Depth Averaged $k-\varepsilon$ Turbulence Model for the Computation of Free Surface Flow, *Journal of Hydraulic Research*, Vol 32, 1994, No.3, PP. 415-444.
[7] Harten, A., High resolution schemes for hyperbolic conservation laws, *J. Comput. Phys., 49, 357, 1983.*
[8] Harten, A., Engquist B., Osher S., and Chakravarthy S., Uniformly high-order accurate essentially nonoscillatory schemes, III, *J. Comput. Phys. 71, 231 1987.*
[9] Henderson F, Open channel flow, *Maxmillian (1966)*
[10] Jameson, A, Schmidt, W. & Turkel E., Numerical Solution of the Euler Equations by Finite Volume Method Using Runge – Kutta Time Stepping Schemes, *AIAA Paper, 81-1259, June 1981.*
[11] Jiang, GS. and Shu CW., Efficient implementation of weighted ENO schemes, *J. Comput. Phys. 126, 202, 1996.*
[12] Jiang, G.S. and C.-C. Wu, A high-order WENO finite difference scheme for the equations of ideal

magneto hydrodynamics, *Journal of Computational Physics,150, 561-594, 1999.*
[13] Kleb WL, Btina JT and Williams MH, Temporal adaptive Euler/Navier Stokes algorithm involving unstructured dynamic meshes, *AIAA Journal 30, 8, 1980-1985,1992*
[14] Liggett, JA, *Fluid Mechanics*, McGraw-Hill, Inc (1994).
[15] Liu, X.-D., S. Osher and T. Chan, Weighted essentially non-oscillatory schemes, J. *Comput. Phys, 115, 200, 1994.*
[16] Lin GF, Lai JS, Guo WD. Finite-volume component-wise TVD schemes for 2D shallow water equations. *Adv Water Resource 2003;26:861–73.*
[17] M.E. Hubbard, P. Garcia-Navarro, Flux difference splitting and the balancing of source terms and flux gradient, *J. Comput. Phys.165 (2000) 89.*
[18] Morris, M. (ed.), 2nd CADAM Meeting Proceedings, *HR Wallingford, 2/3 March (1998).*
[19] Mingham CG, Causon DM. Calculation of unsteady bore diffraction using a high resolution finite volume method. *J Hydraul Res 1998;38:49–56.*
[20] Nelida Crnjaric –Zic, Senka Vukovic, Luka Sopta, Balanced finite volume WENO and central WENO schemes for the shallow water and the open-channel flow equations, *Journal of Computational Physics,(2004).*
available online at www.sciencedirect.com
[21] Osher S, Solomone F, Upwind difference schemes for hyperbolic systems of conservation law, *Math Computat 1982;38:339–74.*
[22] P. Garcia -Navarro, M.E. Vazquez-Cendon, On numerical treatment of the source terms in the shallow water equations, *Comput.Fluids 29 (2000) 951.*
[23] Shao, Z. Y., S. Kim and S. A. Yost, A portable numerical method for flow with discontinuities and shocks, *Proceedings of 17th Engineering Mechanics Conference, ASCE, June 13-16, University of Delaware, Newark, DE, USA, Paper 65 (on CD), 2004.*
[24] Toro, E, Riemann Solvers and Numerical Methods for Fluid Dynamics, *Springer Verlag, Berlin (1999).*
[25] Thierry Gallouet, Jean-Marc Herard, Nicolas Seguin, Some approximate Godunov schemes to compute shallow-water equations with topography, *Computers & Fluids 32 (2003) 479–513, www.elsevier.com/locate/compfluid*
[26] Vaserio Caleffi, Alessandro Valiani and Andrea Zanni, Finite volume method for simulating extreme flood events in natural channels, *Journal of Hydraulic Research Vol. 41, No. 2 (2003), pp. 167–177.*
[27] Whitham, G.B. (1974), Linear and Nonlinear Waves, *J.Wiley & Sons*.
[28] Zhao DH, Shen HW, Tabios III GQ, Lai JS, Tan WY. A finite volume two-dimensional unsteady flow model for river basins. *J Hydraul Eng ASCE 1994;120:863–83.*
[29] Zhao DH, Shen HW, Lai JS, Tabios III GQ. Approximate Riemann solvers in FVM for 2D hydraulic shock modelling. *J Hydraul Eng ASCE 1996;122:692–702.*